DTU Library

A non-dimensional time-domain lumped model for externally DC biased capacitive microphones with two electrodes

Printezis, Georgios; Aage, Niels; Lucklum, Frieder

Published in:
Applied Acoustics

Link to article, DOI:
10.1016/j.apacoust.2023.109758

Publication date:
2024

Document Version
Publisher's PDF, also known as Version of record

Applied Acoustics 216 (2024) 109758

Contents lists available at ScienceDirect

Applied Acoustics

journal homepage: www.elsevier.com/locate/apacoust

A non-dimensional time-domain lumped model for externally DC biased capacitive microphones with two electrodes

Georgios Printezis [a,*], Niels Aage [b], Frieder Lucklum [a]

[a] Centre for Acoustic-Mechanical Microsystems (CAMM), Department of Electrical and Photonics Engineering (Electro), Technical University of Denmark (DTU), DK-2800 Kgs. Lyngby, Denmark

[b] Centre for Acoustic-Mechanical Microsystems (CAMM), Department of Civil and Mechanical Engineering (Construct), Technical University of Denmark (DTU), DK-2800 Kgs. Lyngby, Denmark

ABSTRACT

Microphones that utilize externally biased capacitive transduction (condenser microphones) are typically being modeled in lumped parameter networks where the mechanical, acoustical, and electrical elements are all represented as passive electronic circuit components. Those models have been shown to be insufficient to fully describe crucial aspects of this type of transducer, such as the pull-in phenomenon in which, after a certain distance and for a certain bias voltage, the moving electrode, typically a flexible membrane, attaches itself to the stationary. In this paper, we account for several non-linearities present in an extended simplified model of such a transducer in the time domain and identify the different factors related to its nonlinear response. We derive a time-domain non-linear non-dimensional system of equations for the coupled lumped model where we also take into account parasitic capacitances that are usually present and can significantly affect the overall electroacoustic performance as well as the fringing fields due to the nonhomogeneous electric field between the electrodes and nonlinearities related to damping due to the thin-film of air between the electrodes. We present the nondimensionalization method we used that allows for the identification of a novel set of nondimensional parameters that characterize the non-linear behavior of our system in the time-domain. A designer can use these parameters to optimize for linearity in the voltage response of the transducer. We post-process our time-domain solution to calculate the response to the fundamental excitation frequency and discuss the harmonic distortion. It is shown that coupling the electrical nonlinearities to the mechanical can significantly contribute to the nonlinear voltage response of the transducer. Our model agrees well with nonlinear measurements of analog microelectromechanical (MEMS) microphones for a set of physical values of the nondimensional parameters.

1. Introduction

Microphones that incorporate externally biased microelectromechanical (MEMS) sensors, commonly known as MEMS microphones (MEMSM), are complex System-in-Package (SiP) devices that consist of a transduction element, the sensor, along with dedicated circuitry responsible for charging the electrodes of the transducer that also afford signal conditioning and read-out capability mounted on a printed circuit board (PCB) that is covered by a metallic lid attached to it. Traditionally, such a complex system is modeled using analog mechanoelectroacoustic networks where the total behavior is described as the interplay of all the related physical domains, i.e., the mechanical, electrical, and acoustical [22]. Depending on the analogy, each domain consists of the relevant elements represented by passive electrical components, such as resistors, capacitors, and inductors. The energy transfer from one domain to another is modeled by transformers or gyrators with adequate turn ratios.

The type of modeling described in the preceding paragraph can be very efficient in calculating the total response of the system for a limited frequency range and can provide a systems-level physical overview of the device operation. These models can also be used in combination with other modeling techniques where the response of the transducer is simulated by such a network and other parts of the system, such as gaskets and vents that form the acoustical path to the device, are simulated in more elaborate ones, utilizing methods such as the finite element (FEM) and boundary element (BEM).

Capacitive Micromachined Ultrasonic Transducers (CMUTs) are another type of capacitive transducers frequently mentioned in the literature [21,18,15]. While CMUTs may share some similarities in design with typical MEMS microphones, they operate at significantly higher frequencies and have much smaller dimensions. CMUTs and capacitive microphones exhibit distinct specifications in terms of sensitivity, frequency and dynamic range.

* Corresponding author.
E-mail addresses: geopr@dtu.dk (G. Printezis), naage@dtu.dk (N. Aage), fluc@dtu.dk (F. Lucklum).

https://doi.org/10.1016/j.apacoust.2023.109758
Received 22 March 2023; Received in revised form 9 November 2023; Accepted 19 November 2023
Available online 14 December 2023

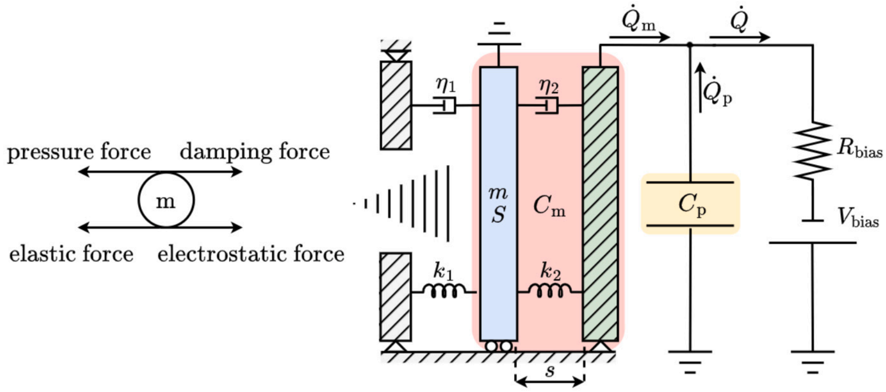

Fig. 1. Analog electromechanical network of a parallel plate capacitive transducer. The circle with the adjacent arrows represents the point mass of the moving electrode. The parasitic capacitance (C_p) is placed in parallel to the capacitance formed by the electrodes of the transducer (C_m). The DC source (V_bias) and the resistor in series to the latter (R_bias) charge both parallel capacitances.

In this paper, we derive a time domain lumped model of capacitive microphones that also takes into account the charging and discharging of electrodes when biased with a DC voltage source and a resistor. The use of such a basic charging network aims for a conceptual understanding of the charging operation in relation to the electroacoustic performance of the device. Previous research on a similar time-domain model [10] indicates that such models can describe additional aspects and phenomena that cannot be modeled with network models. A phenomenon that is being neglected in the circuit models is that of the *pull-in* instability [13], namely a physical phenomenon by which when a certain voltage is applied at a certain distance of the electrodes the electrostatic forces become so large that the elastic forces in the system are no longer capable of keeping the two electrodes apart as they rapidly collapse into one another. We expand upon such a model by also including parasitic capacitances usually present in such devices that are a combination of regions in the sensor element that do not respond to acoustic pressure and can also include the input capacitance of the following amplification stage [17,16]. We also take into account the thin film of air between the electrodes to the device's operation, the fringing fields due to the nonhomogeneous electric field between the electrodes, and the amount and number of perforations. We do not use FEM and BEM methods as these methods are more useful for specific geometries and materials which are not the subject of this work. The assumptions made in this paper are the ones made in most lumped models of condenser microphones.

We finally go a step further by performing a technique called nondimensionalization that is used in modeling MEMS devices which is a process by which we transform a system of equations into one that has normalized nondimensional variables [9,12]. With it, the various variable quantities of the system are combined and related to its basic elements. This allows us to identify the parameters that relate to the different sources of nonlinearity, i.e. sources that are directly related to the nonlinear voltage response of the transducer, and enables the characterization of the system in terms of these parameters that describe sets of systems with relatively equal behavior. Computationally, the non-dimensional systems can be much more well-posed and less prone to divergence due to numerical errors. Finally, and most importantly, nondimensionalization reduces the parameter space allowing for a more concise representation of the system.

2. The nondimensional dynamical system

Here we present the nondimensionalization method we used that allows for the identification of a novel set of nondimensional parameters. We use the method to nondimensionalize the equation that describes the forces acting on the moving electrode and the equation that describes the charging. This allows us to identify a novel set of parameters that relate to the nonlinear response of the system. The main factors identified are λ which was related to the nonlinearities due to the *softening* of the elastic force and couples the charging to the mechanical behavior of the moving electrode, the nondimensional parasitic capacitance, c_p, which was related to the uneven distribution of charge to the electrodes and the parasitics, the impedance factor, τ_0, which acts as damping to the fluctuation of the total charge stored in the transducer, and σ which acts as a factor to the nonlinear thin-film damping. Finally, the fringing field factor χ, and the perforated area ratio A were found to contribute to the nonlinear response.

Making a number of assumptions with regard to the operation of a miniature microphone, the authors in [10] make a comparison between a dynamic model of the transducer to an equivalent circuit model. Doing a frequency domain analysis on both representations and by comparison they identify the relationship between the physical parameters in them. The mechanical compliance of the diaphragm is identified as being the reverse of its lumped stiffness. The total damping factor is identified as being the sum of the radiation resistance and the resistances that correspond to the viscous losses in the air gap between the electrodes and backplate holes. Finally, the equivalent mass is identified as being the sum of air radiation and diaphragm mass. The air compliance between the two electrodes is considered as being negligible due to the highly perforated backplate. In their analysis they observed that the pull-in instability is not represented in the case of the equivalent circuit. Extending upon such a model we derive the time-domain nondimensional ordinary differential system of equations that completely describe its response to an impinging pressure force to the moving electrode.

As shown in Fig. 1 the electrodes are charged using a resistor (R_bias) in series to the electrodes and the DC bias voltage (V_bias). The parasitic capacitance which includes the capacitance formed by the conductive elements in an actual transducer as well as the input capacitance of the following amplification stage (C_p) is placed in parallel to the electrodes. The moving electrode that has a mass m and area A is at a distance s from the stationary of the same area and together they form the capacitance C_m. The damping in the displacement of the moving electrode is assumed to be mostly related to the energy dissipation due to the air movement between the electrodes and through the backplate holes with viscous damping coefficient η_2 and due to radiation of air with viscous damping coefficient η_1. The elastic forces acting on the moving electrode are due to the air in the backchamber of the transducer with mechanical stiffness k_2 and its mechanical support with mechanical stiffness k_1.

Taking into account all the forces acting on the moving electrode, namely the acoustic force, the electrostatic force, the viscous force, the elastic force, and the charging of the electrodes, as well as capacitances that do not respond to acoustic pressure [17] (which from now on we will be referring to as *parasitic*), we built a nonlinear nondimensional

Table 1
Dimensional Quantities.

Symbol	Expression	Unit (S.I.)	Definition
t'	-	s	time
m	-	Kg	mass of moving electrode
g	-	m/s^2	gravitational acceleration
k	-	N/m	linear stiffness due to the mechanical support of the moving electrode
s	-	m	instantaneous distance between the electrodes
s_0	-	m	initial distance between the electrodes
s_e	-	m	distance between the electrodes at equilibrium
S	-	m^2	total electrode area
V	-	V	instantaneous voltage across the moving and the stationary electrode
V_{bias}	-	V	bias DC voltage
f	-	1/s	frequency of impinging pressure
ω	$2 \cdot \pi \cdot f$	1/s	angular frequency of impinging pressure force
ω_n	$\sqrt{k/m}$	1/s	natural frequency of undamped mass-spring oscillator
ρ_{air}	-	kg/m^3	density of medium (air)
R	-	m	radius of the moving electrode
t_{bp}	-	m	thickness of stationary electrode
c_{snd}	-	m/s	speed of sound
μ	-	kg/m s	viscosity of medium (air)
V_{bc}	-	m^3	volume of air in the backchamber
ε	-	F/m	electrical permittivity of air
F_p	-	N	pressure force acting on the moving electrode
L_{bc}	V_{bc}/S	m	length of air in the backchamber
C_0	$\varepsilon \cdot S/s_0$	F	initial capacitance formed by the electrodes without taking into account the perforations
Q_0	$V_{bias} \cdot (\chi_0 \cdot (1-A) \cdot C_0 + C_p)$	C	initial charge stored on both the electrodes taking into account the perforations, the parasitics, and the fringing fields

system of ordinary equations that describes the dynamical operation of the biased mass-spring system. The equations are presented in the most economical and physically meaningful way. Detailed derivation and discussion will be given in subsequent sections.

The nondimensional *force equation*:

$$\boxed{\ddot{w} = \rho - 2 \cdot \left(\sigma \cdot \zeta_{film} \cdot \frac{1}{w^3}\right) \cdot \dot{w} + \kappa_{bc} \cdot (w_e - w) + (1-w) + \lambda \cdot v^2 \cdot \frac{d c_m}{d w},} \tag{1}$$

The nondimensional *current equation*:

$$\boxed{\tau \cdot \dot{q} = -(v-1)} \tag{2}$$

The nondimensional *voltage equation*:

$$\boxed{v = q \cdot w \cdot \frac{\chi_0 \cdot (1-A) + c_p}{\chi \cdot (1-A) + c_p \cdot w}} \tag{3}$$

The nondimensional *impedance factor*:

$$\boxed{\tau = \tau_0 \cdot (\chi_0 \cdot (1-A) + c_p)} \tag{4}$$

In the preceding equations, the following substitutions have been made,

$$\omega_n = \sqrt{\frac{k}{m}},\ t = \omega_n \cdot t',\ w = \frac{s}{s_0},\ \lambda = \left(\frac{1}{2} \cdot \frac{\varepsilon \cdot S \cdot V_{bias}^2}{s_0^2}\right) \cdot \left(\frac{1}{k \cdot s_0}\right),$$

$$\Omega = \frac{\omega}{\omega_n},\ \zeta_{film} = \frac{3 \cdot \mu \cdot S^2}{4 \cdot \pi \cdot \sqrt{m \cdot k} \cdot s_0^3},\ G(A) = \frac{A}{2} - \frac{A^2}{8} - \frac{\ln A}{4} - \frac{3}{8},$$

$$\theta = \frac{8 \cdot G(A)}{N},\ \sigma = \frac{\theta}{1+\theta},\ L_{bc} = \frac{V_{bc}}{S},\ \kappa_{bc} = \frac{\rho_{air} \cdot c_{air}^2 \cdot S}{k \cdot L_{bc}},$$

$$C_0 = \frac{\varepsilon \cdot S}{s_0},\ c_m = \frac{C_m}{C_0},\ \rho = \frac{F_p}{k \cdot s_0},$$

$$v = \frac{V}{V_{bias}},\ Q_0 = V_{bias} \cdot \left(\chi_0 \cdot (1-A) \cdot C_0 + C_p\right),\ q = \frac{Q}{Q_0},$$

$$c_p = \frac{C_p}{C_0},\ \tau_0 = \omega_n \cdot R_{bias} \cdot C_0,$$

where k (N/m) is the mechanical stiffness of the linear elastic force acting on the moving electrode, t' (s) is the dimensional time, s_0 (m) is the initial distance of the electrodes in the absence of electrostatic force, ω is the frequency of the impinging pressure force, ρ_{air} (kg/m^3) is the density of air, R is the radius of the moving electrode, t_{bp} is the thickness of the backplate, c_{snd} (m/s) is the speed of sound, μ (kg/m s) is the viscosity of air, A is the fraction of the perforated area, N is the number of perforations, V_{bc} (m^3) is the volume of air in the backchamber, ε (F/m) is the electrical permittivity of air, F_p (N) is the pressure force acting on the moving electrode, V (V) is the voltage across the moving and the stationary electrode, and χ is the correction factor to the capacitance formed by the electrodes due to the fringing fields [6], and χ_0 is the fringing field correction at distance s_0. For convenience we present the dimensional and nondimensional quantities in Tables 1 and 2 respectively.

In our model we are assuming that,

$$\boxed{m << \frac{k \cdot s_0}{g}} \tag{5}$$

where m (kg) is the mass of the moving electrode, and g (m/s^2) is the gravitational acceleration. This means that we are assuming that the weight of the moving electrode, and thus the system's orientation, does not contribute significantly to the total force acting on it. We should also point out that a fundamental assumption made in the model is that $\omega \cdot R << c_{snd}$ which for the dimensions of small capacitive transducers means roughly that for the excitation frequency

$$\boxed{f < 10\ \text{kHz}} \tag{6}$$

Finally, our model does not take into account any deformation in the moving electrode due to the impinging pressure force. This can be viewed as a more direct representation of a very stiff diaphragm with spring support. What we show in this paper is that there can be other

Table 2
Nondimensional Quantities.

Symbol	Expression	Definition
t	$\omega_n \cdot t'$	time
w	s/s_0	instantaneous distance between the electrodes
w_e	s_e/s_0	distance between the electrodes at equilibrium
λ	$\varepsilon \cdot S \cdot V_{\text{bias}}^2/2 \cdot k \cdot s_0^3$	factor that couples the mechanical nonlinear response to the charging
Ω	ω/ω_n	frequency of impining pressure force
r	$8 \cdot \rho_{\text{air}} \cdot (\omega_n \cdot R)^3/3 \cdot k$	radiation mass component
ζ_{rad}	$\rho_{\text{air}} \cdot \omega_n^2 \cdot S^2/4 \cdot \pi \cdot \sqrt{m \cdot k} \cdot c_{\text{snd}}$	radiation damping ratio
ζ_{film}	$3 \cdot \mu \cdot S^2/4 \cdot \pi \cdot \sqrt{m \cdot k} \cdot s_0^3$	thin-film damping ratio
A	-	ratio of the perforated area over the total area of the electrode
$G(A)$	$A/2 - A^2/8 - (\ln A)/4 - 3/8$	-
N	-	number of perforations (holes)
θ	$8 \cdot G(A)/N$	-
σ	$\theta/(1+\theta)$	thin-film damping factor
κ_{bc}	$\rho_{\text{air}} \cdot c_{\text{air}}^2 \cdot S/k \cdot L_{\text{bc}}$	stiffness factor due to the volume of air in the backchamber of the device
c_m	C_m/C_0	capacitance formed by the two electrodes
ρ	$F_p/k \cdot s_0$	pressure force impinging on the moving electrode
v	V/V_{bias}	voltage across the moving and the stationary electrode
q	Q/Q_0	charge stored in the electrodes and the parasitics
c_p	C_p/C_0	parasitic capacitance
τ_0	$\omega_n \cdot R_{\text{bias}} \cdot C_0$	impedance factor
χ	-	correction factor to the capacitance formed between the two electrodes due to the fringing fields
χ_0	-	correction factor due to the fringing fields at the initial distance s_0
χ_e	-	correction factor due to the fringing fields at the equilibrium distance s_e

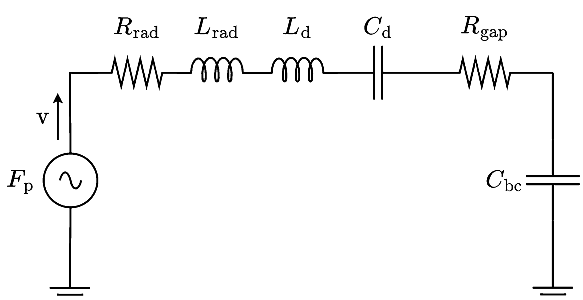

Fig. 2. Circuit equivalent linear system in the impedance analogy of the mechanical force acting on the moving electrode. The circuit fully describes the *small-signal* response of the mass-spring system in Fig. 1. C_d should not be confused with C_m which is the instantaneous electrical capacitance formed by the electrodes.

sources of nonlinearities other than those related to mechanical deformation.

Fig. 2 represents the proposed equivalent linear system in the impedance analogy of the mechanical force acting on the moving electrode similarly to [7,8]. We omit the mass and compliance of the volume of air between the electrodes assuming that the number and rate of the perforations are large enough. Since we model the movement of the membrane for a rigid backplate the velocity (v) induced by the pressure force (F_p) that flows through all the mechanical components is the same and thus is placed in series. R_{rad} is the mechanical radiation resistance, and L_{rad} is the mass of the radiating air, i.e., when the device is operated in reverse as a loudspeaker. $C_d = C'_d/\nu$ is the compliance of the moving electrode, where C'_d is the compliance due to the mechanical support of the moving electrode and ν is the spring softening factor explained in section 2.4. L_d is the mass of the moving electrode. R_{gap} is the mechanical resistance caused by air streaming through slits and holes in the narrow air gap between the diaphragm and the backplate, and L_{gap} is the respective air mass that is considered negligible in our calculations. C_{bc} is the compliance of the volume of air enclosed in the backchamber of the device. C_d should not be confused with C_m which is the instantaneous electrical capacitance formed by the electrodes. We should also mention that we assume that there is only one moving electrode thus assuming that the compliance and mass of the rigid, i.e. the backplate, is large enough.

A more extensive mechanical impedance lumped element representation of a parallel plate capacitive microelectromechanical (MEMS) microphone is proposed in Fig. 3. Here we are taking into account the viscous damping (R_{in}) and mechanical air mass (L_{in}) of the inlet as well as the mechanical compliance (C_{fc}) of the front chamber, the mechanical mass of the air between the electrodes (L_{gap}), the mechanical mass (L_{bp}) and compliance (C_{bp}) of the backplate, and the mechanical viscous damping (R_{vent}) and air mass (L_{vent}) in the pressure equalization path. The force acting on the diaphragm is the force across the volume of air in the front chamber, and thus it is represented grounded. The mass and compliance are placed in parallel to the viscous damping and mass of air in the airgap as the force that squeezes the air between the electrodes is exerted on the backplate. The pressure force across the compliance of the front chamber is the pressure force acting on the moving electrode. That force is impeded at the lower frequencies as the fluctuation of the density of air becomes so slow that gradually becomes identical on both sides of the moving electrode as the vibrating mass in the ventilation path becomes lower. A steady state and dynamic analysis of this complete circuit is beyond our scope of investigation. We assume that the frequencies we are interested in are high enough so that ventilation does not affect our system, and the resonator formed by the mass, compliance, and damping of the inlet and the front chamber is decoupled from the movement of the electrode.

2.1. Nondimensional force equation

In Fig. 1 the stiffness between the electrodes, k_2, represents mainly the compliance of the volume of air enclosed in the backchamber, the air space between the transduction element, and the rigid walls of the metallic lid. The mechanical stiffness due to the electrode's support is represented as a linear elastic force with stiffness k. Additionally, the total viscous force between the electrodes with damping coefficient η_2 is assumed to be mainly due to the *thin-film damping*. In the nondimensionalization process that follows the capital F refers to dimensional force whereas small f refers to nondimensional force component. The time-derivatives are taken with respect to the dimensional time for the equations that give the dimensional force, and the non-dimensional time for the equations that give the nondimensional force.

According to Newton's second law, the rate of change of the momentum in an inertial system must be equal to the total sum of the forces,

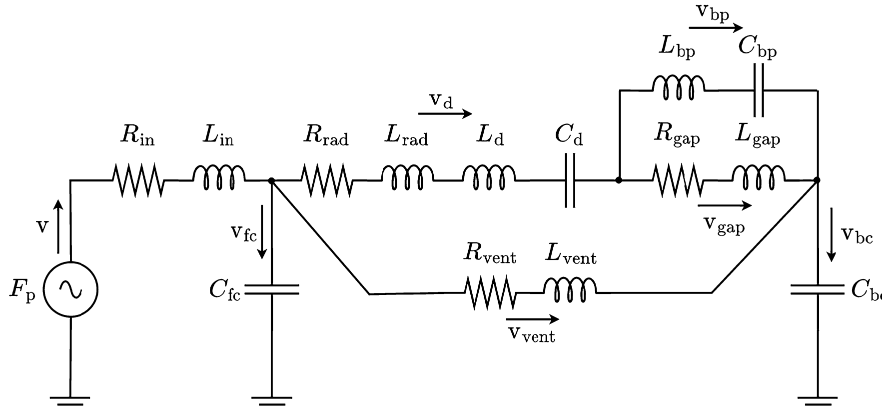

Fig. 3. Mechanical impedance lumped element representation of a parallel plate capacitive microelectromechanical (MEMS) microphone that includes the front chamber and the ventilation path. The circuit should be regarded as a physical extension of Fig. 2, which includes the effect of additional geometrical entities in the path to the sensor element on the input pressure force.

$$F_{tot} = \dot{M}, \tag{7}$$

where M (kg m/s) is the momentum of the system. We formulate our system in terms of the relative distance between the electrodes as in this way we are able to refer to the relative contraction and expansion of that distance instead of relying on a system of reference. The maximum linear elastic force towards the stationary electrode due to the mechanical support of the moving electrode is

$$F_{el,max} = k \cdot s_0, \tag{8}$$

where s_0 is the initial distance of the electrodes in the absence of the electrostatic force, and k (N/m) is the stiffness of the linear elastic force due to the mechanical support of the moving electrode. Also, the time variable, t' (s), is nondimensionalized by the natural frequency of the mass-spring oscillator, ω_n (1/s),

$$t = \omega_n \cdot t'. \tag{9}$$

Nondimensionalizing equation (7) with (8) and (9) we obtain,

$$f_{tot} = \ddot{w} \tag{10}$$

where $f_{tot} = f_p + f_{visc} + f_{el} + f_{es}$, where f_p, f_{es}, f_{visc}, and f_{el}, are the nondimensional pressure, electrostatic, viscous, and elastic forces.

The motivation for nondimensionalizing using equation (8) comes from the fact that the transducer is meant to be operated far below its resonance in a region that is commonly termed as stiffness controlled for a mass-spring oscillator. Nondimensionalizing with the maximum elastic force appears quite natural in that sense as the nondimensional parameters will be scaled with a characterizing quantity. In the following sections, the nondimensionalization of the forces will be shown in more detail.

2.1.1. Nondimensional elastic force

The volume of air behind the transducer that is enclosed in the *backchamber* can be used as a control parameter to the stiffness of the elastic force acting on the moving electrode. In Fig. 1 the compliance of the air between the electrodes is assumed insignificant and so the contribution of the air in the backchamber to the total compliance dominates the operation. We should note that in our model we are assuming that the pressure force is impinging only on one side of the moving electrode. This is in part realized by the existence of the backchamber that keeps the other side of the transducer insulated from sound field propagation in higher frequencies. For an ideal gas, an approximation to the mechanical stiffness associated with the volume of air (V_{air}) in the backchamber can be calculated by the following formula [8,14],

$$k_{bc} = \frac{\rho_{air} \cdot c_{snd}^2 \cdot S^2}{V_{bc}}. \tag{11}$$

We can define the length of the air as $L_{bc} = V_{bc}/S$, and the previous equation can be written with respect to it instead of the volume,

$$k_{bc} = \frac{\rho_{air} \cdot c_{snd}^2 \cdot S}{L_{bc}} \tag{12}$$

In our dynamical model, we assume that any displacement of the electrodes is much smaller than L_{bc}, i.e.

$$\boxed{s_0 << L_{bc}} \tag{13}$$

The total elastic force acting on the moving electrode will be,

$$F_{el} = k_{bc} \cdot (s_e - s) + k \cdot (s_0 - s). \tag{14}$$

The elastic force acting on the moving electrode due to the volume of air in the backchamber is responding to the electrode displacement from the equilibrium distance due to pressure equalization.

Nondimensionalizing with equation (8) we obtain,

$$f_{el} = \kappa_{bc} \cdot (w_e - w) + 1 - w, \tag{15}$$

where

$$\kappa_{bc} = \frac{\rho_{air} \cdot c_{snd}^2 \cdot S}{k \cdot L_{bc}}, \tag{16}$$

2.1.2. Nondimensional damping force

The viscous damping acting on a moving mass varies proportionally to its instantaneous velocity, $\dot{s}$,

$$F_{visc} = -\eta \cdot \dot{s}. \tag{17}$$

The minus sign indicates that for positive velocities for the relative distance between the electrodes, the viscous force has a contracting action. As already discussed η represents the damping coefficient which is mostly due to effects related to the contraction of the volume of air between the electrodes, η_2.

The mechanical viscous damping due to the thin film of air between two disc electrodes with no walls on the sides can be approximated by [3,5],

$$\eta_{film} = \frac{3 \cdot \mu \cdot S^2}{2 \cdot \pi} \cdot \frac{1}{s^3}, \tag{18}$$

where μ (kg/ms) is the medium's viscosity.

If either the moving or the stationary electrode is perforated the damping can be reduced as the air that is getting *squeezed* between them

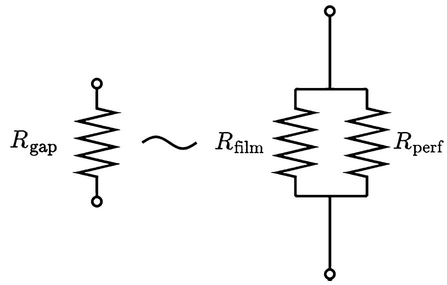

Fig. 4. Mechanical resistance of the airgap between the electrodes is approximated by mechanical resistance of the thin film damping due to the streaming of the air from the sides of two parallel disk elements ($R_{\text{film}} = \eta_{\text{film}}$) in parallel to the mechanical resistance related to the streaming of the air through the perforations ($R_{\text{perf}} = \eta_{\text{perf}}$) [5].

will be able to escape exclusively through the holes. The mechanical viscous coefficient in this case is approximated by [2,4,5,7],

$$\eta_{\text{perf}} = \frac{12 \cdot \mu \cdot S^2 \cdot G(A)}{N \cdot \pi} \cdot \frac{1}{s^3}, \tag{19}$$

in which

$$G(A) = \frac{A}{2} - \frac{A^2}{8} - \frac{\ln A}{4} - \frac{3}{8}, \tag{20}$$

where N is the number of holes on the perforated electrode and A is the ratio of the perforated over the total area. The damping between two discs becomes more important when the perforation area and the number of holes is small as the air flows through a limited area from the sides of the electrodes. The ratio representing the relative importance of the two is defined as,

$$\theta = \frac{\eta_{\text{perf}}}{\eta_{\text{film}}} = \frac{8 \cdot G(A)}{N}. \tag{21}$$

An approximate expression that gives the total damping between the electrodes for when sound can propagate either through the perforations or through side slits in a realistic setting can be mechanically represented as two dampers in series [5]. Eventually, the damping coefficient between the electrodes is approximated by (see Fig. 4),

$$\frac{1}{\eta} = \frac{1}{\eta_{\text{film}}} + \frac{1}{\eta_{\text{perf}}}. \tag{22}$$

Nondimensionalizing the viscous damping force in equation (17) using equations (8) and (9) we obtain,

$$f_{\text{visc}} = -2 \cdot \sigma \cdot \zeta_{\text{film}} \cdot \frac{1}{w^3} \cdot \dot{w}, \tag{23}$$

where $\zeta_{\text{film}} = 3 \cdot \mu \cdot S^2 / 4 \cdot \pi \cdot \sqrt{m \cdot k} \cdot s_0^3$. In the equation, we have introduced the σ parameter which acts as a factor to the nonlinear damping related to the thin film of air between the electrodes,

$$\sigma = \frac{\theta}{1 + \theta}. \tag{24}$$

In Fig. 5, θ is given in a contour diagram with respect to the number of perforations (N) and the ratio of the perforated over the total area (A). In the same figure, a logarithmic graph of σ with respect to θ is presented. We observe depending on the desired performance not only does the perforated area need to be large enough but the number of perforations also needs to be significant. The desired amount of perforations and perforated area to obtain a specified σ parameter value can be extracted from these graphs.

We should mention here that more elaborate lumped models of dissipation for perforated microelectromechanical systems already exist in the literature [11,19] but dealing with them would defeat the purpose of practical conceptual understanding of the nonlinear dissipating effects to the response of our system.

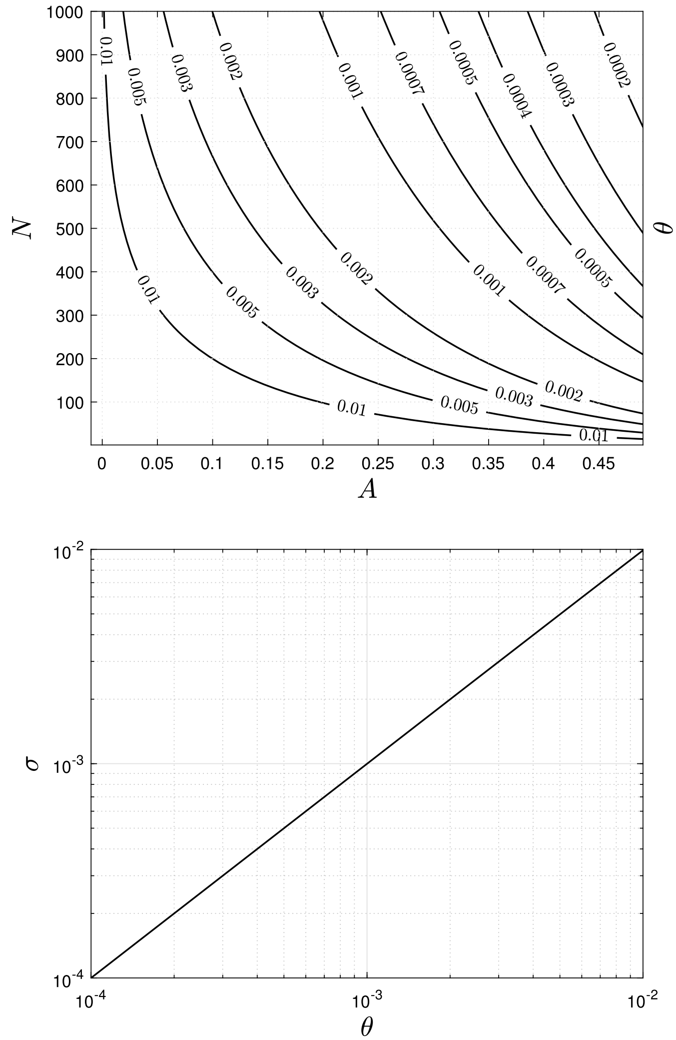

Fig. 5. On the top plot a contour graph of the ratio of damping coefficients due to the thin-film damping (θ) with respect to the number of perforations (N) and the ratio of the perforated area (A) is presented from equation (21). On the bottom plot, the factor to the thin-film damping (σ) is shown with respect to θ from equation (24). The smaller the value of σ the better in relation to the nonlinear response as σ is a factor to the nonlinear thin-film damping term.

On a final note when the pressure force seizes to impinge on the moving electrode it is reasonable to expect that no further oscillation should be occurring and the dynamical system should directly obtain its equilibrium. This is true in a mass-spring oscillator for constant values of ζ over unity. As we will be discussing in a later section the relative distance between the electrodes can only be over 2/3 of the total initial distance in the absence of electrostatic force. Imposing both of the preceding bounds we obtain the following expression for the values of θ,

$$\frac{1}{\frac{27}{8} \cdot \zeta_{\text{film}} - 1} < \theta < \frac{1}{\zeta_{\text{film}} - 1}. \tag{25}$$

At the same time as we can observe in equation (23) large values for the thin-film damping factor increase the nonlinear effects related to it. Thus, around an equilibrium distance ζ should be close to the critical value for an optimal response minimizing nonlinearities. For critical damping at lower frequencies near the *operation distance*, i.e. the relative distance at equilibrium,

$$\sigma \approx \frac{w_e^3}{\zeta_{\text{film}}} \tag{26}$$

Thus, for a given relative distance at equilibrium the value of θ for near critical damping in lower frequencies is given by,

$$\theta \approx \frac{w_e^3}{\zeta_{\text{film}} - w_e^3}. \tag{27}$$

2.1.3. Nondimensional electrostatic force

The electrostatic force exerted on the electrodes of the transducer due to the induced charge from the biasing network is given by [22],

$$F_{\text{es}} = \frac{1}{2} \cdot V^2 \cdot \frac{dC_{\text{m}}}{ds}, \tag{28}$$

where C_{m} is the capacitance formed by the electrodes having a distance s from each other.

Nondimensionalizing with equation (8) we obtain,

$$f_{\text{es}} = \lambda \cdot v^2 \cdot \frac{dc_{\text{m}}}{dw}. \tag{29}$$

In the preceding equation, we have introduced the following parameter [9],

$$\lambda = \left(\frac{1}{2} \cdot \frac{\varepsilon \cdot S \cdot V_{\text{bias}}^2}{s_0^2}\right) \cdot \left(\frac{1}{k \cdot s_0}\right), \tag{30}$$

where ε, and S are the permittivity of air, and the area of the moving electrode respectively. This parameter represents the ratio of the electrostatic force acting on the moving electrode if the initial distance from the stationary in the absence of the electrostatic force is retained, over the maximum linear elastic force that would be acting on the moving electrode towards the stationary. For given dimensional characteristics this factor can be controlled by applying the appropriate biasing voltage. In our model, the parameter functions as a factor to the nonlinear electrostatic force acting on the moving electrode.

Observing that $c_{\text{m}} = \chi \cdot (1 - A)/w$, where χ is the correction factor due to fringing fields,

$$f_{\text{es}} = -\lambda \cdot v^2 \cdot \frac{\chi \cdot (1 - A)}{w^2}. \tag{31}$$

Notice that since $\chi > 1$ for any separation of the electrodes, the fringing fields increase the amount of contribution of the electrostatic force and essentially the nonlinearities related to it.

2.1.4. Nondimensional pressure force

The sound pressure impinging on the moving electrode is modeled here as a pressure load exerted on the area of the latter,

$$F_{\text{p}} = S \cdot p. \tag{32}$$

Nondimensionalizing with equation (8) we obtain,

$$\rho = \frac{S}{k \cdot s_0} \cdot p. \tag{33}$$

For a periodic signal, we can write

$$p = \sum_i P_i \cdot \sin(\Omega_i \cdot t + \phi_i), \tag{34}$$

where P_i is the amplitude of the impinging acoustic pressure component.

2.2. Nondimensional current equation

The charge on the electrodes is induced by a DC voltage source, V_{bias}, in series with a resistor, R_{bias}. The readout is assumed to be taking place across and through the electrodes of the transducer with the biasing scheme in Fig. 6. According to *Kirchhoff's Voltage Law* (KVL) the equation that describes the flow of charge from the electrodes can be written as,

$$R_{\text{bias}} \cdot \dot{Q} = R_{\text{bias}} \cdot \left(\dot{Q}_{\text{m}} + \dot{Q}_{\text{p}}\right) = -(V - V_{\text{bias}}), \tag{35}$$

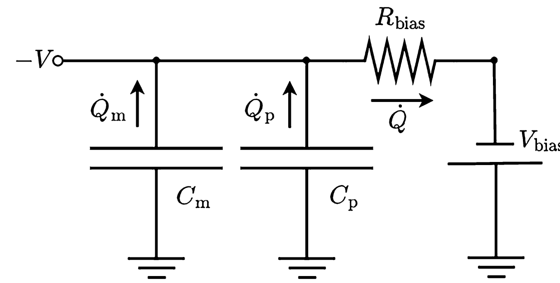

Fig. 6. Charging Circuit to the transducer. The circuit corresponds to the charging of the mass spring system in Fig. 1.

where V, $\dot{Q}_{\text{m}}$, and $\dot{Q}_{\text{p}}$, are the voltage across, and the current through the electrodes and the parasitic capacitance parallel to them. Since the voltage across the electrodes fluctuates around the biasing voltage the minus sign indicates that a positive flow of charge is related to a voltage that is lower than the bias.

Nondimensionalizing with the bias voltage and equation (9) we obtain equation (2), restated here for convenience,

$$\tau \cdot \dot{q} = -(v - 1),$$

where as stated in equation (4),

$$\tau = \tau_0 \cdot (\chi_0 \cdot (1 - A) + c_{\text{p}}).$$

It can be observed that as τ becomes very small the voltage across the electrodes remains relatively constant for any relative displacement induced by an impinging pressure. Conversely, as τ becomes larger the fluctuation of charge is dampened and the induced charge on the electrodes remains relatively constant for any relative displacement.

2.3. Nondimensional voltage equation

The voltage applied across the electrodes is also applied across the parasitics formed in parallel to them (see Fig. 6). So, the voltage is obtained as,

$$V = \frac{Q_{\text{m}} + Q_{\text{p}}}{C_{\text{m}} + C_{\text{p}}}.$$

Nondimensionalizing with the bias voltage we obtain equation (3),

$$v = q \cdot w \cdot \frac{\chi_0 \cdot (1 - A) + c_{\text{p}}}{\chi \cdot (1 - A) + c_{\text{p}} \cdot w},$$

where χ is the correction factor due to the fringing fields [6], and A the perforation ratio [2].

It can be shown that the relative total positive charge concentration can be written as the addition of the relative positive charge stored in the transducer and the relative positive charge stored in the parasitic capacitance normalized by the total charge,

$$q = q_{\text{m}} + q_{\text{p}}, \tag{36}$$

where the nondimensional charge concentration on the positively charged electrode is,

$$q_{\text{m}} = \frac{v}{w} \cdot \frac{\chi \cdot (1 - A)}{\chi_0 \cdot (1 - A) + c_{\text{p}}}, \tag{37}$$

and the nondimensional charged concentration on the positively charged parasitic capacitance is,

$$q_{\text{p}} = v \cdot \frac{c_{\text{p}}}{\chi_0 \cdot (1 - A) + c_{\text{p}}}. \tag{38}$$

From these equations, we can observe that increasing the parasitic capacitance increases the charge on it which is only dynamically related to the voltage across the electrodes, and decreases the charge on the latter. We can also see that as the parasitic capacitance becomes relatively larger and larger the fluctuation of voltage as well as the fluctuation of charge are diminishing and any relative displacement of the electrodes will not induce any output. Finally, we can observe that increasing A increases the charge on the parasitics.

2.4. Equilibrium state analysis & the pull-in phenomenon

An equation that relates the λ parameter, to the nondimensional equilibrium distance, w_e, can be derived from equations (1) and (31),

$$\lambda = \frac{w_e^2}{\chi_e \cdot (1-A)} \cdot (1-w_e), \tag{39}$$

where χ_e is the correction factor due to the fringing fields [6] at equilibrium, and A is the perforation ratio [2].

Note that at equilibrium the voltage across the electrodes will be the same as the bias, meaning that $v_e = 1$. We can now identify that the maximum value for λ is,

$$\lambda_{PI} = \frac{1}{\chi_e \cdot (1-A)} \cdot \frac{4}{27}, \tag{40}$$

at which point the distance between the electrodes is

$$w_{PI} = \frac{2}{3}. \tag{41}$$

Notice that the fringing fields decrease the maximum value of this factor for the same *pull-in distance* as has been observed previously. This means that not taking into account the fringing fields λ and essentially the pull-in voltage are overestimated. The same happens when A is increased. To show that this maximum point has a physical meaning and that it is effectively the point under which no equilibrium can be established we can take a closer look at these equilibrium states. Near such a state the potential of the system will be at its minimum and thus its dynamic behavior can be approximated by an equivalent stiffness; a linear force to the displacement of the electrodes. Eventually, the factor to that stiffness can straightforwardly be obtained by our nondimensional equations at, or close enough, an equilibrium distance. It can be shown that the factor by which the linear elastic force acting on the moving electrode is reduced, or *softened*, at equilibrium is,

$$\nu = 3 - \frac{2}{w_e}, \tag{42}$$

where w_e represents the normalized ratio of the total distance at equilibrium over the initial distance of the electrodes in the absence of electrostatic force. What this factor represents is mainly that the restoring force in the system is a combination of the elastic and electrostatic forces. Since the device being modeled is meant to be operated far below its resonance, in a region that is mainly stiffness controlled, in terms of a mass-spring oscillator, the biasing voltage allows control over its performance. The evident trade-off is the one we are trying to quantify, which is the nonlinearities related to this *tuning*.

From equations (30) and (42) it can be shown that,

$$\lambda = \frac{4}{\chi_e \cdot (1-A)} \cdot \frac{1-\nu}{(3-\nu)^3} \tag{43}$$

In Fig. 7 we observe that for negative values of ν, i.e. when $w_e < w_{PI}$, the "effective" elastic force becomes negative, meaning that the total force is now exerted to the moving electrode towards the stationary, and the *pull-in* phenomenon occurs, as the electrodes rapidly attach to one another. From equation (42) we observe that for the pull-in nondimensional distance, w_{PI}, $\nu = 0$. In a mass-spring system with a dissipation mechanism like the one we are dealing with, random thermal agitation of air molecules near the surface of the moving electrode [1,5] will create a form of broadband input noise. This can be represented in our system as a time-dependent forcing term that would depend on the damping coefficient, $F_n = F_n(t';\ \eta)$. When our system is

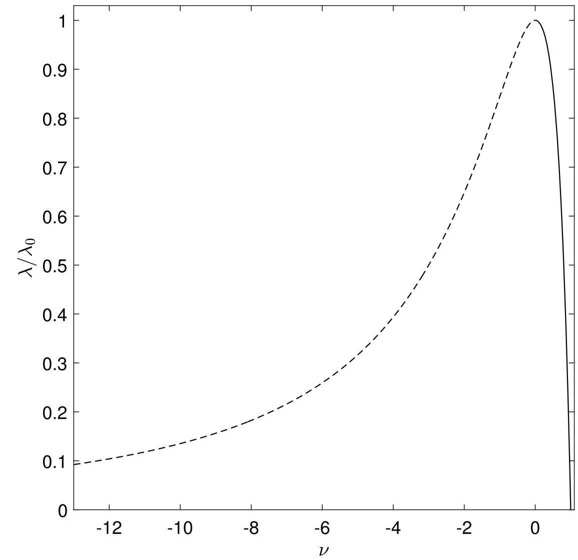

Fig. 7. The graph shows the λ factor normalized by its maximum value λ_0 with respect to the *softening* factor, ν. The solid line represents *operational* region, i.e. the region in which $\nu > 0$. In the graph we are assuming that the effect of the fringing fields is negligible, i.e. $\chi/\chi_0 \approx 1$.

at a metastable state any amount of force can cause the electrodes to collapse into one another as the pull-in phenomenon will occur. This means that any equilibrium point will be larger than the precedingly calculated pull-in distance,

$$w_e > w_{PI} \implies \nu > 0. \tag{44}$$

2.5. Readout and amplification stage

To prevent the output signal of the transducer from being affected by the load impedance an amplifying stage that acts as an impedance converter is necessary. Depending on the readout quantity a charge amplifier or voltage amplifier can be used (see Fig. 8). In both cases the *open-circuit* output signal, i.e. the output signal when the transducer is not connected to any load, is a voltage.

In the next section, we obtain the response of the system in terms of the output voltage V_{oc} for both amplification schemes and calculate the total harmonic distortion (*THD*) as follows,

$$THD_x = \frac{\sqrt{V_{oc,2}^2 + V_{oc,3}^2 + V_{oc,4}^2 + \dots}}{|V_{oc,1}|}, \tag{45}$$

where $V_{oc,1}$ is the output signal amplitude at the fundamental frequency, $V_{oc,i}$ is the output signal amplitude of the i^{th} harmonic, and x can be either of V or Q depending on the amplification scheme used at the output stage of the system. Nonlinear transient effects related to the operation of the amplification stage are not taken into account in our model.

3. Comparing with an axisymmetric numerical model

A lumped model construct with similar geometric properties and assumptions is compared with a similar axisymmetric model in COMSOL Multiphysics. Fig. 9 shows the construct and its equivalent mechanical impedance network with nondimensional parameters $\lambda = .02$, $\sigma = .12$, $N = 1$, $c_p = 1.2$, $\tau_0 = 5000$, that is simulated for $\rho = .0002, .0015, .0154$ and $\Omega = .0005, .005, .05$, and assuming that the mechanical stiffness of the backchamber is negligible.

The *mixed* simulation takes place in the frequency domain with a lumped representation of the charging network using the Electri-

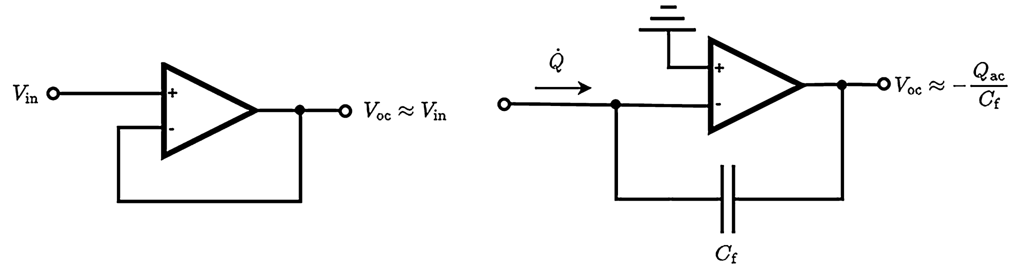

Fig. 8. Voltage (left) and charge (right) amplifiers and their respective voltage output. The charge amplifier acts as an integrator of the input current.

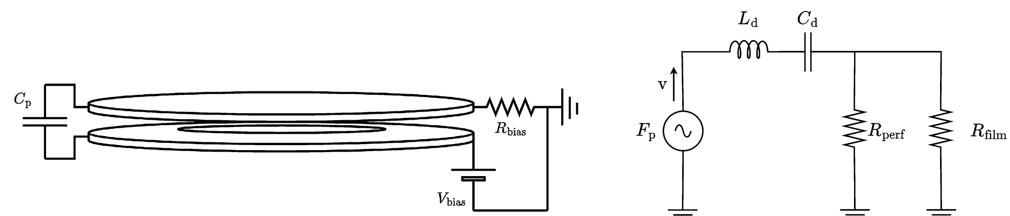

Fig. 9. Mixed model sketch simulated in COMSOL Multiphysics (left), and its equivalent mechanical impedance network (right).

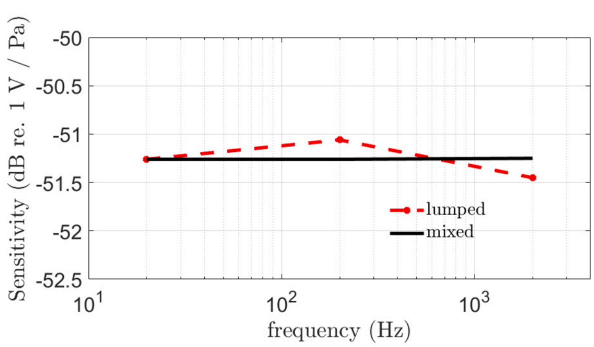

Fig. 10. Calculated sensitivities for the lumped model and the mixed model that combined FEM with lumped model representation for the charging circuit. The sensitivities are calculated for an excitation frequency at 20Hz, 200Hz, and 2kHz. There were no observable differences in sensitivity for different pressure levels of excitation up to 120dB SPL.

cal Circuit Interface. The Membrane interface controls the diaphragm's structural behavior, i.e., as a pre-stressed membrane. The material prescribed for the Membrane is Polysilicon from the built-in library of COMSOL. The electrostatic force is provided by the Electrostatic interface. Finally, the Thermoviscous Acoustics interface is used to describe the movement of the air as the vibrating membrane acts on it (utilizing the Thermoviscous Acoustic-Structure Boundary multiphysics interface). Air is assumed in the space between the electrodes and the perforations (as chosen from the built-in materials library in COMSOL). The sensitivity of the FEM model is fitted to the calculated sensitivity of the lumped model at 20 Hz, applying the appropriate initial stress on the diaphragm. See Fig. 10.

The results show that the calculated sensitivities of the lumped model are in very good agreement with the ones of the finite element model for the same frequencies and pressure levels. The deviation can be attributed to the more elaborate models of the diaphragm and the acoustics in the structure used in COMSOL Multiphysics. More specifically, in the lumped model, the diaphragm is assumed to be a moving piston with a prescribed linear mechanical stiffness, and the Thermoviscous Losses are considered to be only viscous in nature, excluding any inertial or compressibility effects.

4. Comparing with measurements & discussion

To show that our system of equations represents a valid model of a miniature microphone device, such as a MEMS microphone, we use nonlinear measurements on such a device from literature [20] and show that for a set of physical parameters, our model agrees well with those measurements. The authors in [20] use a setup that consists of a loudspeaker, the device under test, and a reference microphone enclosed in a box. They implement a method of harmonic correction to ensure that a pure harmonic acoustic pressure is reproduced in the loudspeaker during the measurements aiming at measuring the nonlinear response occurring when the system is excited with a single harmonic pressure signal.

They excite the measurement system at three frequencies (20 Hz, 200 Hz, 2 kHz) and at twenty sound levels (linear intervals from 90 to 128 dB SPL). They later post-process their measurements, and present their results in the form of graphs of applied sound pressure level and measured for the first three harmonics occurring in the measured signal from the device under test, i.e. the fundamental, the 2$^{\rm nd}$, and 3$^{\rm rd}$ harmonic (shown in Figs. 11, 12, and 13 respectively for each excitation frequency).

In the figures, the measurements from the literature are shown along with the results from the model. The model was fitted to the response of the fundamental at 90 dB, and a set of physical values to the parameters shows that the nonlinear response of such a system can describe the nonlinear response of the measured device at a certain excitation level range. In our model and since the excitation frequencies are much lower than the natural frequency of the mass-spring system we assume that the effects due to radiation are not significant. The higher the impinging pressure force on the moving electrode the higher its relative displacement and as it comes closer to the stationary electrode the electrostatic forces increase. Thus, the average distance is reduced causing additional mean charging to the electrodes. Additionally, initially, the system is in equilibrium and requires some time until it obtains its steady transient, i.e. time-dependent, state. Those transient effects are discarded in post-processing. We also assume that the electrodes are sufficiently close and thin so that the correction factor to the capacitance due to fringing fields is very close to unity ($\chi \approx 1$). For low acoustic pressure levels the higher harmonics responses are below the noise level of the measurement system and since we are not modeling the noise a good much those low levels is not observed. Finally, in our fitting, we assume that $\kappa_{\rm bc} << 1$ and that the backchamber mainly functions as an insulator to

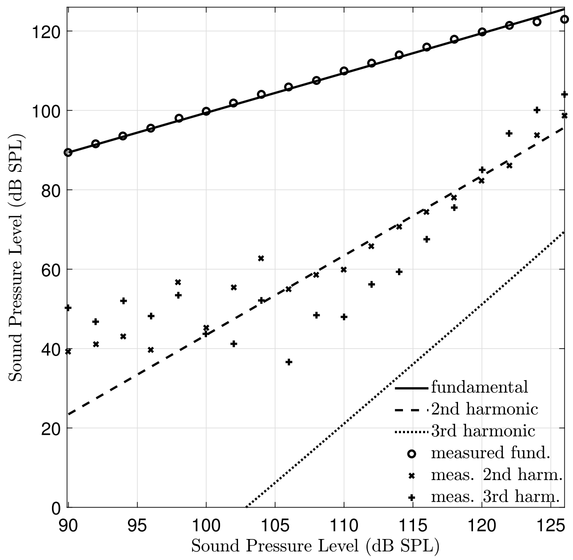

Fig. 11. Pressure response of the model (*y-axis*) with respect to the applied pressure (*x-axis*) compared with the response of the measurements presented in [20] at 20 Hz.

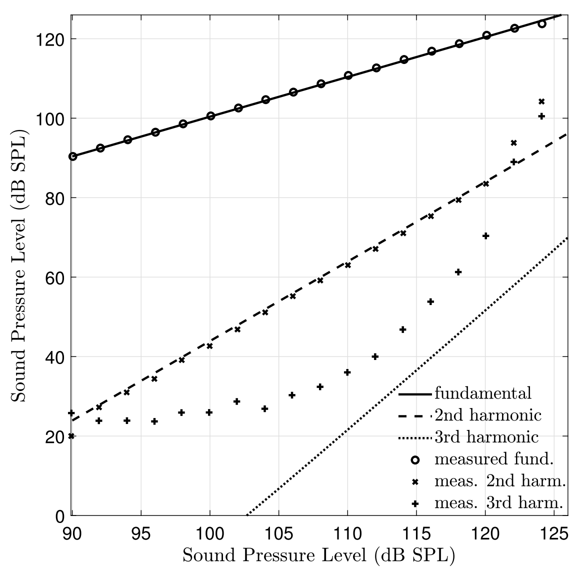

Fig. 12. Pressure response of the model (*y-axis*) with respect to the applied pressure (*x-axis*) compared with the response of the measurements presented in [20] at 200 Hz.

the sound field. In all of the figures $\lambda = .041$, $\zeta_{\text{film}} = 24.8$, $\tau_0 = 5000$, $c_\text{p} = 1.2$, $\sigma = .036$, and $N = 46$.

At 20 Hz ($\Omega = 5.4\text{e}{-4}$) a good match can be observed for the fundamental and the second harmonic but the measured third harmonic is excited at higher levels than predicted by the model. This can be due to the model not taking into account the effects related to acoustic wave propagation on both sides of the membrane.

At 200 Hz ($\Omega = 5.4\text{e}{-3}$) a relatively good match can be observed between the levels of 105 dB to 120 dB SPL. Over 120 dB SPL an increased response to the higher harmonics can be observed indicating the presence of other nonlinear effects in the measurement system that are not described in this model.

At 2 kHz ($\Omega = 5.4\text{e}{-2}$) the response is relatively similar to the one at 200 Hz. An even better match can be observed between 105 and 120 dB SPL. Over that range, an increased response in the higher harmonics is observed, as in the other frequencies. This relative increase in the

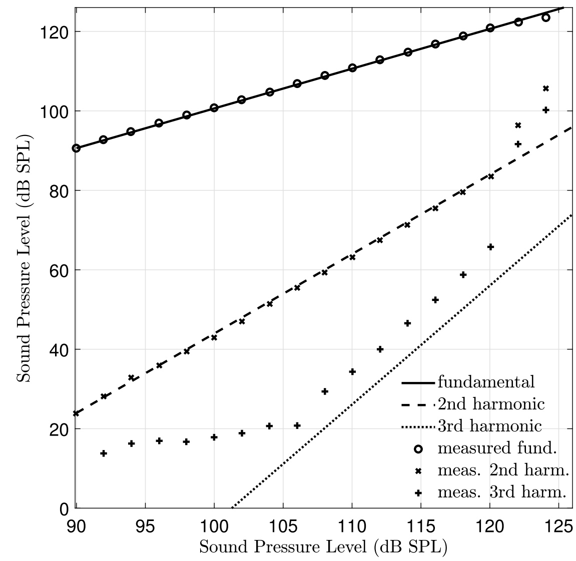

Fig. 13. Pressure response of the model (*y-axis*) with respect to the applied pressure (*x-axis*) compared with the response of the measurements presented in [20] at 2 kHz.

higher harmonics seems to be accompanied by a relative decrease in the fundamental over 120 dB SPL which is common in all measured frequencies.

As already mentioned in a previous section the electrostatic force controls the effective elastic force acting on the moving electrode. The factor ν associated with this was defined in equation (42) and was related to the λ parameter which acts as a nonlinear coefficient in the force equation that describes the response of the moving electrode to an impinging pressure force and is related to the electrical biasing of the system. The nonlinearities related to this parameter will be referred to as mechanical nonlinearities although clearly, the dynamic operation of the system transcends the purely mechanical nature of these nonlinearities as was shown in equation (31).

A second source of nonlinearities described in the equations comes from the non-dimensional parasitic capacitance in equation (3) with the main factor being the normalized parasitic capacitance, c_p. As the voltage across the terminals of the transducer fluctuates in response to the impinging acoustic pressure, part of the charge stored in the transducer is “consumed” by the parasitic capacitance and causes an uneven distribution of charge between the transducer electrodes and the acoustically “inactive” capacitances. This is illustrated in equations (36), (37), and (38). This causes a nonlinear electrostatic force between the electrodes when the system is dynamically excited. The nonlinearities related to this will be referred to as electrical although as in the previous case, the dynamic operation of the system transcends their purely electrical nature.

To evaluate the significance of these sources of nonlinearities the total harmonic distortion of the fitted model is calculated (Fig. 14) in the absence of the non-linear term in equation (1) by setting $w_\text{e} = 1$, in which case $\kappa = 1$, and $\lambda = 0$, and of the nonlinear term in equation (3) by setting $c_\text{p} = 0$, separately. In Fig. 14 we observe that the coupling of both nonlinear sources can significantly affect the voltage response of the device.

A third source of nonlinearity comes from the fluctuation of charge during the dynamical relative displacement of the electrodes. In Figs. 16 and 17 we show the total harmonic distortion as calculated from the response of the fitted model when excited at 2 kHz for different values of the nondimensional time-constant, τ_0. There we observe that for the whole range of excitation the lower the τ_0 the higher the calculated total harmonic distortion. So, τ_0, which acts as a electrical damping to the fluctuation of charge concentrated on the electrodes, is related to

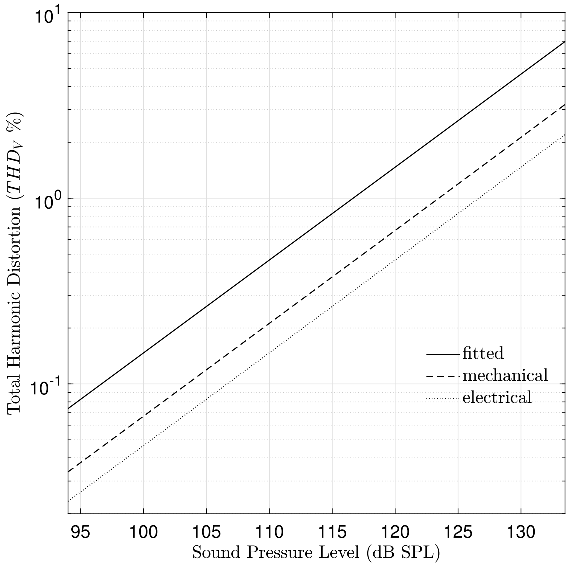

Fig. 14. Total Harmonic Distortion as calculated from the response of the fitted model at 2 kHz, excluding either the mechanical nonlinear component in the non-dimensional force equation (setting $\lambda = 0$), or the parasitic nonlinear component in the nondimensional current equation (setting $c_\mathrm{p} = 0$).

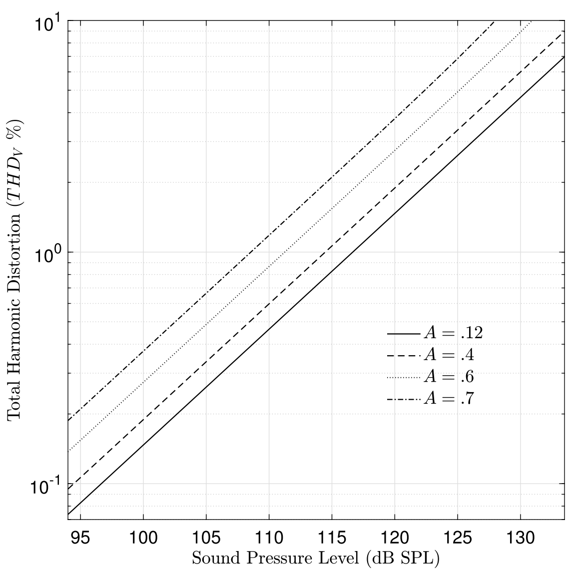

Fig. 15. Total Harmonic Distortion as calculated from the response of the fitted model at 2 kHz, for increasing values of the perforated area ratio (A).

the nonlinearities occurring due to the latter. This parameter can be used to evaluate the desired amount of the biasing resistance needed when the amount of the parasitic capacitance is known, as to minimize the total harmonic distortion. We can also observe that if the final stage is a charge amplifier it appears that ideally and for proper selection of integrating capacitance (C_f) the calculated harmonic distortion is improved compared to a voltage follower.

Finally, a fourth source of nonlinearity comes from the perforated area ratio (A). As can be observed in Fig. 15 increasing this ratio results in increasing the total harmonic distortion. This can be attributed to the increase of charge concentrated on the parasitics and at the same time the decrease of the charge concentrated on the electrodes of the mass-spring system (equations (37) and (38)) as well as the increase of the electrical coupling to the mechanical relative movement of the electrodes (equation (39)).

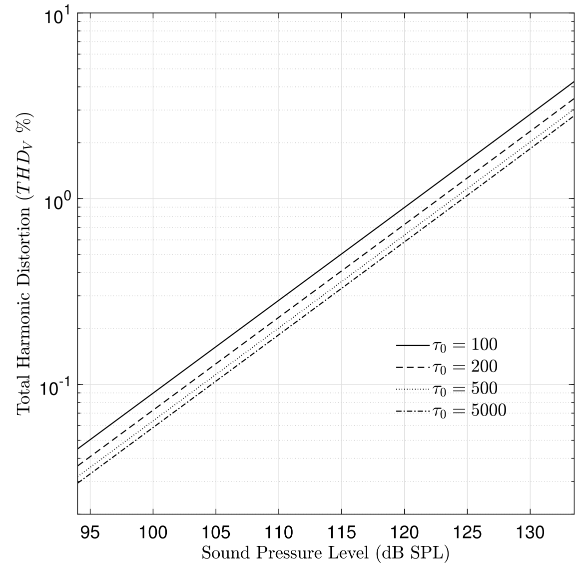

Fig. 16. Total harmonic distortion (THD_V) calculated from the response of the fitted model when excited at 2 kHz for different values of τ_0 setting $c_\mathrm{p} = 0$.

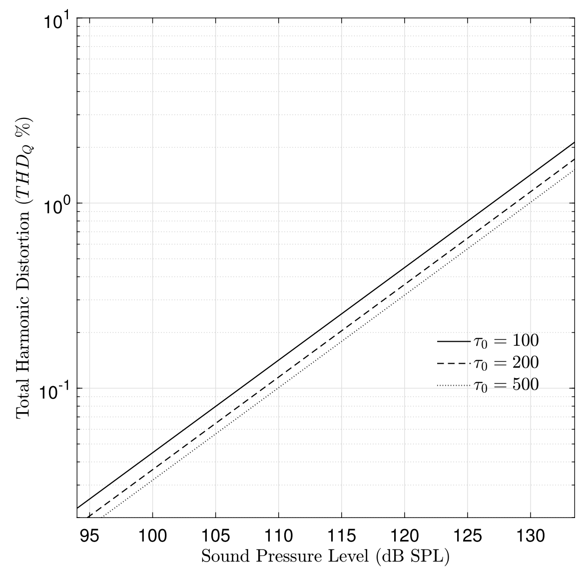

Fig. 17. Total harmonic distortion (THD_Q) calculated from the response of the fitted model when excited at 2 kHz for different values of τ_0 setting $c_\mathrm{p} = 0$.

5. Conclusion

In this paper we model capacitive microphones biased with a DC voltage source and a resistor (condenser microphones) as parallel plate constructs with varying distance responding to an impinging acoustic pressure. A system of nondimensional ordinary differential equations is derived that fully describes the operation of such a construct. We use these equations to account for several nonlinearities present in the time-domain voltage response by calculating the total harmonic distortion for different excitation levels and frequencies. We show that for a set of physical parameters such a model can describe the nonlinear behavior of an actual MEMS transducer. We describe the several factors to the physical quantities that relate to our model's nonlinear response and show how they affect the calculated harmonic distortion relative to the extracted parameters from the fitted model. The main factors identified are λ which is related to the nonlinearities due to the *softening* of the elastic force and which couples the charging to the mechanical behavior of the moving electrode, the nondimensional parasitic capacitance, c_p, which is related to the uneven distribution of charge to the electrodes and the parasitics, the impedance factor, τ_0, which acts as damping to the fluctuation of the total charge stored in the transducer, and σ which acts as a factor to the nonlinear thin-film damping, as well as the fringing field factor χ related to the non-homogeneous electric field between the electrodes, and the perforated area A which are found to contribute to the nonlinear response. The effect of those parameters is described analytically through the derivations found in the text and numerically in the figures where we use the fitted model as a basis to observe the effect of changing those parameters to the nonlinear voltage response. A designer can use these parameters to optimize for linearity in the voltage response of the transducer. We show that the coupling of the electrical nonlinearities to the mechanical can significantly contribute to the nonlinear voltage response of the transducer. Future work will focus on revealing other sources of nonlinearities such as those related to the stretching of the membrane at higher levels of excitation as well as the dynamical movement of the backplate, and evaluating their relevance to the device's voltage response to that of double backplate and diaphragm models.

CRediT authorship contribution statement

Georgios Printezis: Conceptualization, Methodology, Formal analysis, Software, Writing – Original draft preparation, Visualization, Investigation.

Niels Aage: Supervision, Writing – Review & Editing.

Frieder Lucklum: Supervision, Writing – Review & Editing.

Declaration of competing interest

The authors declare that they have no known competing financial interests or personal relationships that could have appeared to influence the work reported in this paper.

Data availability

Data will be made available on request.

Acknowledgements

The author would like to thank Finn T. Agerkvist for his critique on the early modeling efforts and for offering an open and constructive dialogue.

References

[1] Callen Herbert B, Welton Theodore A. Irreversibility and generalized noise. Phys Rev July 1951;83(1):34–40. https://doi.org/10.1103/physrev.83.34.

[2] Skvor Z. On the acoustical resistance due to viscous losses in the air gap of electrotastic transducers. Ultrasonics Jan. 1969;7(1):83. https://doi.org/10.1016/0041-624x(69)90627-1.

[3] Starr JB. Squeeze-film damping in solid-state accelerometers. In: IEEE 4th technical digest on solid-state sensor and actuator workshop. IEEE; 1990.

[4] Bergqvist J, et al. A silicon condenser microphone with a highly perforated backplate. In: TRANSDUCERS '91: 1991 international conference on solid-state sensors and actuators. Digest of technical papers. IEEE; 1991.

[5] Gabrielson TB. Mechanical-thermal noise in micromachined acoustic and vibration sensors. IEEE Trans Electron Devices May 1993;40(5):903–9. https://doi.org/10.1109/16.210197.

[6] Nishiyama H, Nakamura M. Form and capacitance of parallel-plate capacitors. IEEE Trans Compon Packaging Manuf Technol, Part A 1994;17(3):477–84. https://doi.org/10.1109/95.311759.

[7] Scheeper PR, et al. A review of silicon microphones. Sens Actuators A, Phys July 1994;44(1):1–11. https://doi.org/10.1016/0924-4247(94)00790-x.

[8] Pedersen Michael, Olthuis Wouter, Bergveld Piet. A silicon condenser microphone with polyimide diaphragm and backplate. Sens Actuators A, Phys Oct. 1997;63(2):97–104. https://doi.org/10.1016/s0924-4247(97)01532-x.

[9] Pelesko John A, Bernstein David H. Modeling MEMS and NEMS. CRC Press; 2002.

[10] Nadal-Guardia R, Brosa AM, Dehl A. AC transfer function of electrostatic capacitive sensors based on the 1-D equivalent model: application to silicon microphones. J Microelectromech Syst Dec. 2003;12(6):972–8. https://doi.org/10.1109/jmems.2003.820290.

[11] Bao Minhang, Yang Heng. Squeeze film air damping in MEMS. Sens Actuators A, Phys May 2007;136(1):3–27. https://doi.org/10.1016/j.sna.2007.01.008.

[12] Younis Mohammad I. MEMS linear and nonlinear statics and dynamics. Springer US; 2011.

[13] Zhang Wen-Ming, et al. Electrostatic pull-in instability in MEMS/NEMS: a review. Sens Actuators A, Phys Aug. 2014;214:187–218. https://doi.org/10.1016/j.sna.2014.04.025.

[14] Esteves Josué, et al. Lumped-parameters equivalent circuit for condenser microphones modeling. J Acoust Soc Am Oct. 2017;142(4):2121–32. https://doi.org/10.1121/1.5006905.

[15] Maity Reshmi, et al. Analysis of fringing capacitance effect on the performance of micro-electromechanical-system-based micromachined ultrasonic air transducer. Micro Nano Lett June 2018;13(6):872–7. https://doi.org/10.1049/mnl.2017.0688.

[16] Malcovati Piero, Baschirotto Andrea. The evolution of integrated interfaces for MEMS microphones. Micromachines June 2018;9(7):323. https://doi.org/10.3390/mi9070323.

[17] Shubham S, Nawaz M. Estimating parasitic capacitances in MEMS microphones using finite element modeling. In: Excerpt from the proceedings of the 2019 COMSOL conference in Boston; 2019.

[18] Maity Reshmi, Maity Niladri Pratap, Baishya Srimanta. An efficient model of nanoelectromechanical systems based ultrasonic sensor with fringing field effects. IEEE Sens J Feb. 2020;20(4):1746–53. https://doi.org/10.1109/jsen.2019.2948795.

[19] Naderyan Vahid, Raspet Richard, Hickey Craig. Thermo-viscous acoustic modeling of perforated micro-electro-mechanical systems (MEMS). J Acoust Soc Am Oct. 2020;148(4):2376–85. https://doi.org/10.1121/10.0002357.

[20] Novak Antonin, Honz'ık Petr. Measurement of nonlinear distortion of MEMS microphones. Appl Acoust Apr. 2021;175:107802. https://doi.org/10.1016/j.apacoust.2020.107802.

[21] Pal Moumita, et al. Effects of fringing capacitances and electrode's finiteness in improved SiC membrane based micromachined ultrasonic transducers. Microsyst Technol Jan. 2021;27(10):3679–91. https://doi.org/10.1007/s00542-020-05135-7.

[22] Shubham Shubham, et al. A novel MEMS capacitive microphone with semiconstrained diaphragm supported with center and peripheral backplate protrusions. Micromachines 2022;13(1):22. https://doi.org/10.3390/mi13010022.